76th International Astronautical Congress (IAC), Sydney, Australia, 29 September - 3 October 2023.

IAC-25-B4.7.3.100195

Collision risk assessment and avoidance methods for safe autonomous proximity operations

Giacomo Borelli [a,*], Gabriella Gaias[a], Camilla Colombo [a]

[a] *Department of Aerospace Science and Technology, Politecnico di Milano, Via La Masa 34, 20156, Milan, Italy. giacomo.borelli@polimi.it, gabriella.gaias@polimi.it, camilla.colombo@polimi.it*
[*]Corresponding author: giacomo.borelli@polimi.it

Abstract

Various current and planned space missions involve proximity operations between objects in near-Earth space. Ensuring the safety of these operations is critical, particularly for autonomous spacecraft that increasingly rely on minimal ground monitoring and intervention. This work presents novel methods addressing two key functions of flight safety systems: collision risk assessment and avoidance strategies in contingency scenarios. The developed algorithms are designed for autonomous applications, enhancing the robustness and reliability of proximity operations.
Keywords: Proximity Operations, Collision Risk, Collision Avoidance, Autonomy, Safety

1. Introduction

Proximity operations have attracted growing attention in recent years due to their ability to enable advanced mission architectures and applications. For instance, In-orbit Servicing, Assembly and Manufacturing (ISAM) is gaining momentum and is expected to redefine the way space missions are conducted. Moreover, precise close-formation flying with multiple satellites has demonstrated the potential to significantly enhance the scientific and observational return of space missions. Numerous ventures around the globe has been conducted to demonstrate and develop ISAM capabilities: examples are NASA [1, 2], JAXA [3], ESA [4, 5, 6]; and various private entities, among which Astroscale [7], SpaceLogistic/Northrop Grumman [8], OrbitFab [9].

At the same time, spacecraft engaged in proximity operations are often required to function autonomously, with only limited ground monitoring and intervention. This has created the need for systems characterized by a high level of safety and robustness, to prevent undesirable behaviours that could ultimately lead to in-space collisions. Safety in proximity operations can be considered in two distinct phases. The first is the design phase, where the goal is to define nominal relative trajectories that achieve mission objectives while ensuring no collision risk. An example is the design of eccentricity/inclination (E/I) separated trajectories, which guarantee passive safety for proximity flight [10, 2]. The second is the operations phase, where methods and algorithms are employed during the mission to continuously monitor flight safety and to devise mitigation measures in the event of contingencies or failures. This paper focuses on the second aspect—methods and tools for monitoring and guaranteeing flight safety during proximity operations. In this context, two key challenges must be addressed: collision risk assessment and collision avoidance planning and recovery. The first involves strategies to analyse relative trajectories and accurately predict potential collision risks, both in the present and in the future. The second concerns the mitigation actions required when a contingency arises, ensuring that the spacecraft involved can reduce the risk of collision and eventually resume nominal operations.

In literature a plethora of methods for collision risk assessment of in-space objects are available when considering conjunction dynamics for near-Earth objects, which rely on algorithms to compute the probability of collision accounting for nominal orbits and their dispersion at close-encounter [11]. Among these, there are analytical [11] and numerical methods [12, 13, 14, 15] to retrieve the probability of collision of an encounter. However, most of the techniques available for conjunction assessment rely on short term encounters assumptions, where the relative motion is considered rectilinear and fast. This cannot be applied and is not relevant for proximity operations scenario, where the relative orbits of an object with respect to the other evolves slowly together with their dispersion. Collision risk for long-term encounter is in general more complex, as less simplifying assumptions can be introduced, and often more computationally demanding. Often the analysis are performed considering the instantaneous collision probability along the trajectory (or probability rate) [16, 11, 17, 18, 13, 19]. Past work on application of collision checks in proximity can be divided in geometrical and stochastic/probabilistic methods. Geometrical methods rely on distances check between the relative motion and the evolution of its uncertainties to evaluate the risk of collision [20, 5, 21] . Stochastic methods seek to estimate the instantaneous collision probabilities with probabilistic analyses of the position uncertainties distributions [22, 23, 16, 24, 25]. The work of [26] provides a comparison of the distances and probabilistic metrics and shows their correlation in different proximity scenarios. In this paper, novel methods of probabilistic metrics, related to the instantaneous probability of collisions, are proposed accounting for their computational efficiency for onboard applications.

When a contingency or collision risk is detected, an action—typically a manoeuvre—must be executed on the involved objects to mitigate the threat. The design of Collision Avoidance Manoeuvres (CAM) in autonomous proximity operations strongly depends on the mission's relative trajectory and the time available to act. Indeed, when the controlled objects have more time to implement a manoeuvre, the set of reachable escape trajectories expands, and manoeuvres can be optimized for more favourable positions.

If the relative trajectory already embeds a degree of safety (*e.g.*, through E/I separation), avoidance strategies often focus on planning manoeuvres that re-establish such conditions [10, 27, 28, 29, 30]. Conversely, when the trajectory has no inherent safety properties, the design of avoidance actions must be more general. In these cases, pre-computed CAMs along the nominal trajectory, generated during the design phase, can be highly useful for autonomous operations thanks to their computational efficiency and ease of verification [5, 29]. Optimization-based approaches, such as those developed for long-term in-space encounters, can also be applied [23, 16]. However, ensuring sufficient computational efficiency remains essential for onboard implementation. A comprehensive overview of such methods is provided in [31]. In this work, we propose an algorithm for prompt CAM execution that leverages convex optimization methods, which show strong potential for efficient and reliable onboard applications.

The present paper is organised in the following way. Section 2 provides a introduction to the dynamics models exploited for the relative motion modelling. Section 3 provides definitions useful for flight safety development and models. Section 4 describes the development of the stochastic collision risk assessment methods developed and compared in this work. Section 5 presents the collision avoidance methods proposed for close range fast escape manoeuvres in case of contingencies. Lastly, Section 6 draws the conclusions and sets the future development directions.

2. Relative Dynamics

In this work, the relative dynamics of two objects orbiting in proximity around a primary body (e.g., Earth) are parametrised using quasi–non-singular Relative Orbital Elements (ROEs). Denoting the satellites as chief and deputy, the ROEs are defined as functions of the orbital elements of the two objects, as follows:

$$\delta\boldsymbol{\alpha} = \begin{pmatrix} \delta a \\ \delta\lambda \\ \delta e_x \\ \delta e_y \\ \delta i_x \\ \delta i_y \end{pmatrix} = \begin{pmatrix} (a_d - a_c)/a_c \\ u_d - u_c + (\Omega_d - \Omega_c)\sin i_c \\ e_d \cos\omega_d - e_c \cos\omega_c \\ e_d \sin\omega_d - e_c \sin\omega_c \\ i_d - i_c \\ (\Omega_d - \Omega_c)\sin i_c \end{pmatrix} \quad (1)$$

Here, a denotes the semi-major axis, e the eccentricity, i the inclination, Ω the right ascension of the ascending node, ω the argument of pericenter, and u the mean argument of latitude (defined as $u = M + \omega$). The subscripts d and c refer to the deputy and chief orbits, respectively. The first two components of the ROE state represent the relative semi-major axis and the relative mean longitude, while the remaining terms describe the components of the relative eccentricity and relative inclination vectors, which may also be expressed in terms of their respective magnitudes and phases, as follows:

$$\delta\boldsymbol{e} = \delta e \begin{pmatrix} \cos\varphi \\ \sin\varphi \end{pmatrix}, \quad \delta\boldsymbol{i} = \delta i \begin{pmatrix} \cos\theta \\ \sin\theta \end{pmatrix} \quad (2)$$

When the objects are in proximity, linear relative motion models are available which allow for a extremely efficient propagation of the relative states through State Transition Matrices (STM) and convolution matrix as follows:

$$\delta\boldsymbol{\alpha}(t) = \Phi(t_0, t)\delta\boldsymbol{\alpha}_0 + \int_{t_0}^{t} \Phi(t,\tau)\mathrm{B}(\tau)\boldsymbol{u}(\tau)d\tau \quad (3)$$

where the integral, represent the convolution of the control active in the interval (t_0, t), and the B matrix is obtained from Gauss Variational Equations (GVE). Linear models and STMs in function of ROEs have been developed in literature, which include perturbation effects of the orbital motions and cases with eccentric reference orbits [32]. Under these relative dynamics, also the relative state dispersion errors, in the form of covariance of the ROEs state can be propagated linearly through the following equation:

$$\mathrm{P}(t) = \Phi(t_0, t)\mathrm{P}(t_0)\Phi(t_0, t)^{\mathbf{T}} + \mathrm{Q} + \mathrm{P}_m \quad (4)$$

where the matrix P is the state covariance, the matrix Q the process noise matrix which encloses unmodelled effects in the relative dynamics, P_m the matrix which models the inclusion of manoeuvre dispersions with the techniques shown by Gates [33].

In this work, the model used refers to the model applicable to a proximity operations in Low Earth Orbit (LEO), from Gaias et. al [34]. Nonetheless, the CA and CAM methods described will be generally applicable to all the linear models of relative motion. In the assumption of small-separation, linear mapping through Lyapunov transformation is possible between ROEs state and a Cartesian state expressed in the Radial Transversal Normal (RTN) frame [35].

3. Trajectory safety

The robustness of a relative trajectory to off-nominal conditions and contingencies is determined by the spacecraft capability to assess the risk and provide mitigation measures. Before introducing the methods for collision risks assessments and collision avoidance manoeuvres, the following definitions of different types of trajectory safety to measure the level of safety of a trajectory are introduced:

- **Point-Wise Safety (PWS)**: the relative trajectory of the objects guarantee no collisions between them at at time t_i.
- **Passive Abort Safety (PAS)**: the relative trajectory of the objects guarantee no collision between them for a ΔT time interval of uncontrolled motion from time t_i.
- **Active Collision Safety (ACS)**: the relative trajectory of the objects guarantee no collision between them for a ΔT time interval from time t_i, after the application of a collision avoidance action.

In the context of proximity operations, PWS safety is useful for checking collision conditions along a relative trajectory. On the other hand, the PAS property guarantees at a given point that a trajectory remains collision-free even in the event of a major failure of one of the objects involved, which will result in an uncontrolled natural evolution of the relative dynamics. This characteristic is highly beneficial for the safe design of proximity trajectories, as it allows for a high level of robustness of the operations even under worst-case scenarios. Finally, ACS aims to provide a trajectory with a level of PAS that can only be achieved through active control of one of the objects, which performs an avoidance manoeuvre. Relative trajectories in proximity operations are often designed with PAS characteristics whenever possible. A common example is the use of PAS trajectories based on the eccentricity/inclination (E/I) vector separation concept using ROEs, which are widely applied for far-to-close range approaches in proximity operations in near-circular orbits [10, 36]. This concept exploits the dynamics of relative motion to ensure future collision avoidance by imposing a minimum separation between the chaser trajectory and the target in the radial–normal (RN) plane. This is achieved by aligning the relative eccentricity vector and the relative inclination vector in parallel. Extensions that relax the strict (anti-)parallel conditions are also available in the literature [37].

Nonetheless, the complexity of certain required trajectories in specific missions and operations, such as forced motions or synchronization, often prevents the exclusive use of the E/I separation concept to guarantee a one-orbit minimum distance in the RN plane. The focus of this paper is therefore on general CA and CAM methods applicable across a wide range of scenarios, including complex forced motion operations.

4. Collision risk assessment

Collision risk for proximity operations is discussed in this section. Consider the Cartesian expression of the relative state of the deputy with respect to the chief, expressed in the RTN frame centred on the chief, denoted as $x(t)$, with dispersion described by the covariance $\mathrm{P}(t)$. A Keep Out Zone (KOZ), accounting for the physical dimensions of both objects and centred at the chief, is also defined. The state $x(t)$ is assumed to follow a Gaussian dispersion, which is reasonable given the linear nature of the relative motion. The collision risk assessment problem is generally concerned with computing the relative trajectory and its dispersion, and evaluating the probability of collision with respect to the KOZ. The general form can be expressed as:

$$PoC = \int_T \iiint_{\mathcal{V}} \frac{\exp\left(-\frac{(\mathbf{r}^{\mathrm{T}}-\boldsymbol{\mu}_r)\mathrm{P}_r^{-1}(t)(\mathbf{r}-\boldsymbol{\mu}_r)}{2}\right)}{(2\pi)^{2/3}\det(\mathrm{P}_r(t)))} dV\, dt \tag{5}$$

Here, $\mathcal{V}$ denotes the volume of the KOZ, and T the duration of the trajectory. The integrand is the time-dependent position probability density function of the multivariate distribution of the relative position $\mathcal{N}(\boldsymbol{\mu}_r, \mathrm{P}_r)$, with mean $\boldsymbol{\mu}_r$ and covariance matrix P_r. Unlike short-encounter models for conjunction assessment, in this case the time variation of the covariance over the considered window further complicates the problem. In proximity operations, considering only the time of closest approach along the nominal trajectory may not provide a sufficient or meaningful approximation, since the evolving (and generally growing) dispersion can result in a higher collision probability at other points along the trajectory where the covariance is larger. Therefore, the use of the Instantaneous Probability of Collision (IPoC) metric, or probability of collision rate, is more appropriate for proximity operations, as it evaluates the relative trajectory and dispersion point-wise. Moreover, in operational scenarios, relying on an IPoC often suffices to determine thresholds for avoidance measures. The IPoC can be expressed as:

$$PoC_I = \iiint_{\mathcal{V}} \frac{\exp\left(-\frac{(\mathbf{r}^{\mathrm{T}}-\boldsymbol{\mu}_r)\mathrm{P}_r^{-1}(t)(\mathbf{r}-\boldsymbol{\mu}_r)}{2}\right)}{(2\pi)^{2/3}\det(\mathrm{P}_r(t)))} dV \tag{6}$$

Therefore, the computation of the IPoC must be carried out along the trajectory and the covariance evolution, and evaluated over an extended time window. However, solving the integral in the above equation numerically is computationally demanding and often not a viable solution for autonomous operations. Simplifications of Equations 5 and 6 are therefore often sought to avoid numerical integration in both short- and long-term encounters.

In this paper, we develop and describe methods to simplify or approximate the solution of Equation 6 to enable implementation in autonomous proximity scenarios. First, we assume that the KOZ geometry can be represented by a quadratic form, such as an ellipsoid around the chief. This assumption is reasonable, as indicated by the definitions of regions in the ESA close proximity operations guidelines [38]. Furthermore, we assume that the distribution of the relative position $\mathbf{r}$ follows a multivariate Gaussian $\mathcal{N}(\boldsymbol{\mu}_r, \mathrm{P}_r)$, consistent with Equation 6. The integral of the position probability density over the ellipsoidal KOZ volume can then be reduced to the probability of a positive-definite quadratic form, as follows:

$$PoC_I = \Pr(\mathbf{r}^{\mathrm{T}}\mathrm{A}\mathbf{r} > C) \tag{7}$$

Here, Pr is the probability operator, **A** is the matrix representing the quadratic form defining the shape and orientation of the KOZ, and C is the constant related to its size. In the limiting case of a spherical KOZ, **A** corresponds to the identity matrix and C to the square of the sphere radius, R^2. The problem of computing the probability in Equation 7 therefore reduces to the characterisation of the distribution of a quadratic form in normal variables with non-zero mean and a general covariance. This results in a generalised non-central chi-squared distribution, which in general has no closed-form expression for either its probability density function (pdf) or cumulative distribution function (cdf). Approximating the distribution functions of a general quadratic form is a well-known problem in statistical research [39, 40]. In the following, different approaches are described and compared for addressing this problem. It should be noted that, in conjunction assessment, the main interest lies in determining the cdf of Equation 7, rather than the pdf, since a point-wise check is required at each point of the trajectory to ensure it lies outside the KOZ region.

4.1 Gamma moment matching

The first method described here comes from the family of methods that seek to approximate explicitly the Equation 7 distribution with known distributions by matching their moments m_i, such as works in [41] and [42]. Here a moment-matching with the Gamma distribution is implemented, where the first two moments are matched between the quadratic form and a Gamma distribution. The Gamma moment matching is selected here thanks to its simplicity and explicit nature. The moments m_i of the quadratic form $\mathbf{r}^T A\mathbf{r}$ can be explicitly derived from the expressions of the k-th cumulant κ_k of the quadratic form as [42]:

$$\kappa_k = 2^{k-1}(k-1)!\left(\mathrm{trace}((\mathrm{AP}_r)^k) + \mu_r^{\mathrm{T}}(\mathrm{AP})^{k-1}\mathrm{A}\mu_r\right) \tag{8}$$

with first four moments that can be expressed as:

$$\begin{aligned} m_1 &= \kappa_1, & m_2 &= \sqrt{\kappa_2} \\ m_3 &= \frac{\kappa_3}{\kappa_2^{2/3}}, & m_4 &= \frac{\kappa_4}{\kappa_2^2} \end{aligned} \tag{9}$$

Here, m_1 is the mean, m_2 the variance, m_3 the skewness, and m_4 the kurtosis of the quadratic form. The Gamma moment-matching method implemented here uses m_1 and m_2 of the quadratic form from Eqs. 9 , matching them with those of a Gamma distribution expressed as Gamma(α, θ), where α and θ are the shape and scale parameters, respectively. Specifically, the parameters of the Gamma distribution are derived as:

$$\alpha = \frac{m_1^2}{m_2}, \quad \theta = \frac{m_2}{m_1} \tag{10}$$

The pdf and cdf of the Gamma(α, θ) are then obtained explicitly and considered as an approximation of the respective function of the quadratic form.

4.2 Saddle point approximation

Moment-matching methods are often imprecise when dealing with quadratic forms with large non-centrality and high skewness. Such cases are common in proximity operations scenarios, where the distribution of the position **r** is nominally far from the chief-centred KOZ. Moreover, moment-matching approximations for such distributions often struggle in the tails, which is critical for conjunction assessment in proximity operations, since ideally the probability of collision should be small in nominal scenarios. To address this, another method is proposed here, which exploits the saddle-point approximation of the quadratic form [43, 44, 45]. This method approximates the pdf and cdf of the quadratic form by working with the cumulant generating function $K(\tau)$ and solving the saddle-point equation $K'(\tau) = q$, where q is the point at which the pdf and cdf are to be approximated. Expressions for the pdf and cdf are then obtained using expansion formulas in terms of the saddle point $\hat{\tau}$. Of particular relevance, the cdf describing the probability of the quadratic form in Equation 7 is approximated through a Lugannani & Rice series (truncated at first order) [45] as follows:

$$\Pr(\mathbf{r}^{\mathrm{T}}\mathbf{A}\mathbf{r} > C) \approx \Psi(w) + \psi(w)\left(\frac{1}{w} - \frac{1}{u}\right) \tag{11}$$

where $w = \mathrm{sign}(\hat{\tau})\sqrt{\hat{\tau}q - K(\hat{\tau})}$ Here, $u = \hat{\tau}\sqrt{K''(\hat{\tau})}$. The functions $\Psi(\cdot)$ and $\psi(\cdot)$ denote the cdf and pdf of the normal distribution, respectively. In summary, this method approximates the IPoC by solving a root-finding problem and using explicit expression formulas. Unlike the moment-matching technique (such as the Gamma distribution explained in the previous section), obtaining the approximation of the full pdf and cdf requires solving the saddle-point equation for each point of the distribution. Nonetheless, in conjunction assessment of relative motion, this is not critical, since only a single point corresponding to the probability of being outside the KOZ is needed.

4.3 Simulation results

In this subsection, the approximation methods introduced previously are evaluated in a proximity operations scenario. Specifically, a relative trajectory with initial state and uncertainty conditions listed in Table 1 is propagated forward in time for six hours (approximately four orbital periods in our scenario). The state and uncertainties are propagated using the STM model of reference [34], which accounts for Earth oblateness and differential drag perturbations. The KOZ is modelled as a spherical volume around the chief with radius R_{KOZ}. The results of the PoC approximations are compared with the numerical computation of the PoC according to Equation 6 via quadrature. Additionally, a comparison of the behaviour of these metrics with respect to the Mahalanobis distance between the chief and the deputy position distribution is provided. The evolution of the relative trajectory of the deputy in the chief-

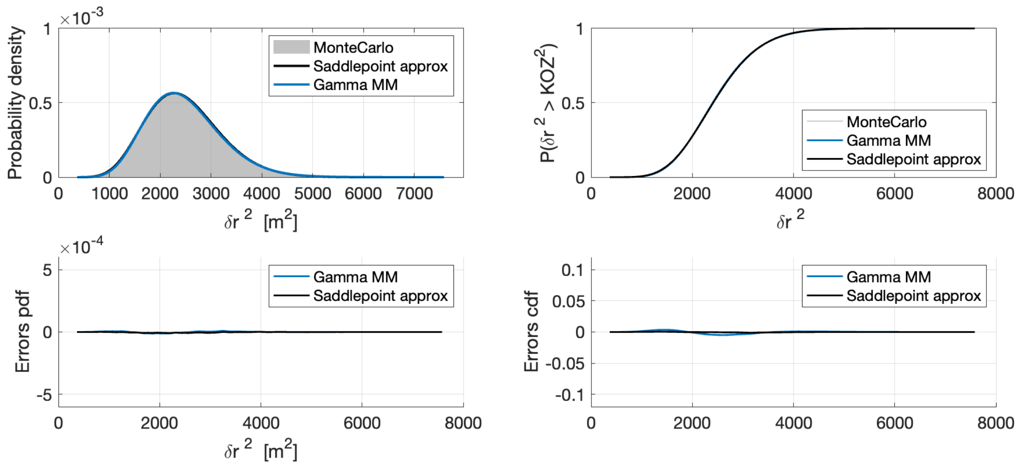

Fig. 1. Results of the quadratic form of relative position distribution approximation through the Gamma moment matching and the saddle point approximation at the time of propagation $t = 0.55$ hours of the collision risk assessment scenario of Table 1. (top-left) Probability density function, (top-right) cumulative distribution function, (bottom-left) absolute error of the pdf with respect to MC sampling, (bottom-right) absolute error of the cdf with respect to MC sampling.

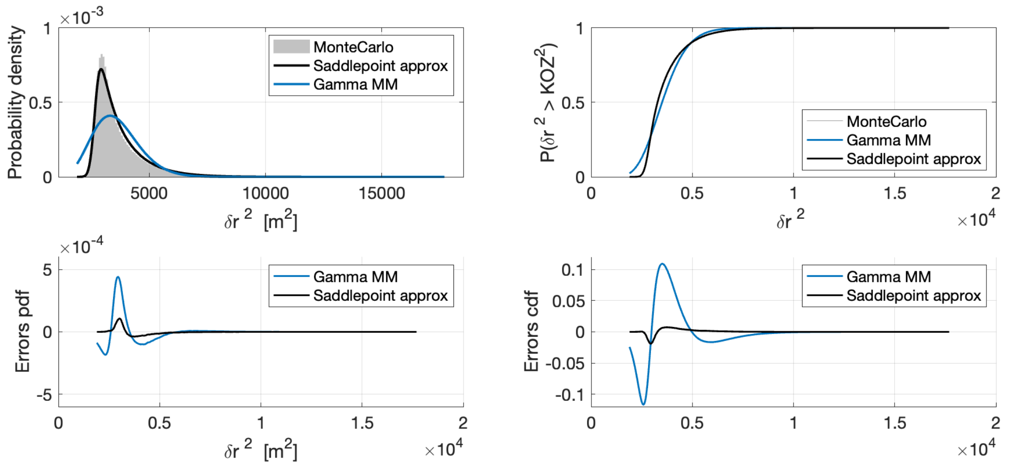

Fig. 2. Results of the quadratic form of relative position distribution approximation through the Gamma moment matching and the saddle point approximation at the time of propagation $t = 1.66$ hours of the collision risk assessment scenario of Table 1. (top-left) Probability density function, (top-right) cumulative distribution function, (bottom-left) absolute error of the pdf with respect to MC sampling, (bottom-right) absolute error of the cdf with respect to MC sampling.

centred RTN frame, along with its dispersion, is shown in Figure 4.

To demonstrate the capability of the methods described in previous sections to approximate the distribution of the quadratic form of the relative position between the deputy and the chief, two different snapshots are compared with Monte Carlo (MC) sampling. Figure 1 shows the approximation of the distance distribution at $t = 0.55$ hours, while Figure 2 shows the results after $t = 1.66$ hours of propagation. From Figure 1, it is evident that both the Gamma moment-matching and the saddle-point approximation are capable of accurately approximating the shape of the pdf and cdf obtained via MC sampling. This snapshot, after a short

Table 1. Parameters for the text case analysed in the CA scenario in proximity operations.

Parameter	Value
$\delta\boldsymbol{\alpha}_0$	[1,20,-15,28,30,40] m
P_0	diag([4,4,4,4,4,4]) m^2
R_{KOZ}	10 m
ΔT_{sim}	6 hours
sma_c	6904692 m
e_c	1e-4
in_c	97.6 deg

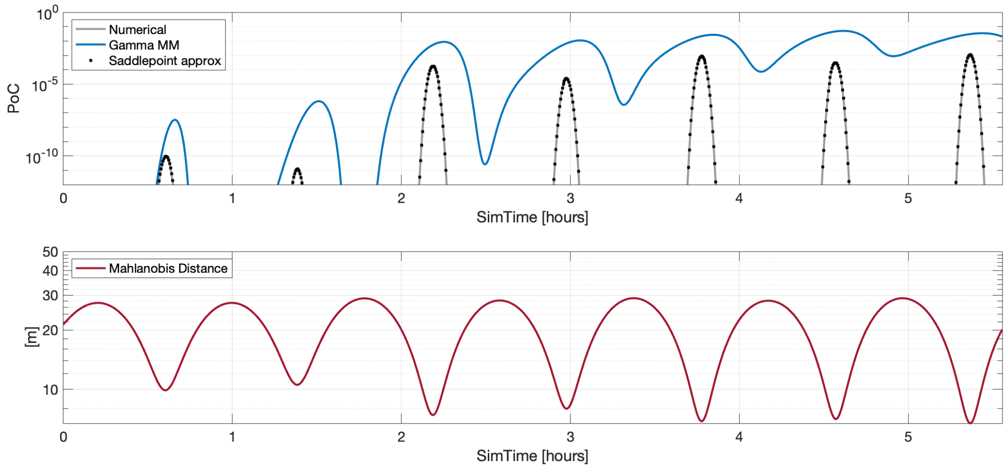

Fig. 3. (Top) Computation of the IPoC with approximation methods and with numerical quadrature for the test case scenario of Table 1. (Bottom) Mahlanobis distance between the chief and deputy considering position uncertainty.

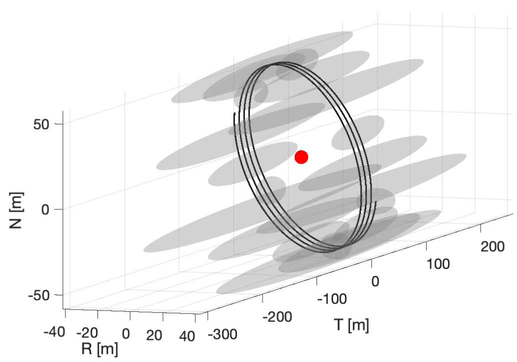

Fig. 4. Relative trajectory of the deputy in the chief RTN frame. In gray the 3σ ellipsoid of the trajectory dispersion are displayed.

propagation time, represents a case where the covariance matrix has not become highly anisotropic, and the skewness of the distribution deviates only slightly from the Gaussian form. Conversely, Figure 2 shows a snapshot in which the covariance is elongated along the along-track direction and the distribution of the quadratic form of the position becomes highly skewed. In this situation, it is apparent that the Gamma moment-matching approximation fails to accurately reproduce the pdf and cdf obtained from MC sampling, whereas the saddle-point method still provides a good approximation. Notably, as can be seen in the bottom plots of Figures 1 and 2, the errors in approximating the pdf and cdf functions are much smaller in the tails of the distributions than near the mean. This is particularly beneficial for collision risk assessment applications, where the computation of small probabilities is often required.

The computation of the IPoC methods along the test case scenario are displayed in Figure 3, together with the IPoC computation by numerically solving the integral of Equation 6 numerically through quadrature. We can note how as propagation time progresses, the explicit analytic approximation of the Gamma moment matching provides larger errors, due to the elongation of the covariance in the along-track direction. On the other hand, the saddle point approximation provides an extremely accurate approximation of the exact IPoC computed numerically. In the bottom plot of Figure 3 the Mahlanobis distance metric between the two objects and their relative position dispersion is displayed, showcasing the capability also of this explicit analytic metric to identify high risk of collision regions.

Table 2. Computational time of the collision assessment of the test case scenario of Table 1.

Method	CPU time
Gamma MM	14.6 ms
Saddle point	195 ms
Numerical	2933 ms
Mahlanobis dist.	12.3 ms

Table 2 reports the computational effort required for the collision assessment checks using the methods described. The reported computational times correspond to the total time needed to evaluate the collision risk assessment algorithms for all 1000 points discretising the propagated trajectory of the scenario. The algorithms are implemented in MATLAB and run on a laptop. The Gamma moment-matching provides a very fast evaluation of collision risks, as it requires only the explicit computation of the Gamma cdf at each point. However, the accuracy of the Gamma approximation quickly degrades over time when the covariance elongates along one direction and the quadratic form distribution of the position becomes highly skewed. In contrast, the saddle-point approximation requires a greater computational effort, as it involves solving a root finding problem to determine the saddle point, along with eigen decomposition computations to ensure the saddle-point equation is well conditioned. Nonetheless, for 1000 evaluations along the trajectory, the CPU time remains below 200 ms, representing more than an order of magnitude improvement compared to the numerical quadrature computation of the IPoC. Finally, the Mahalanobis distance method demonstrates very fast evaluation times, requiring only an eigen decomposition at each step. It is important to note that the computational efficiency of the saddle point based IPoC evaluation along a trajectory can be further improved by performing it only at points where, according to explicit analytic checks such as the Gamma MM or Mahalanobis distance, the risk exceeds a predefined threshold. This hybrid approach allows the IPoC to be refined using the most accurate approximation only when needed, further reducing the computational effort of the collision risk assessment.

5. Collision avoidance

When a contingency or a collision risk is detected during operations, mitigation actions to prevent collision in proximity must be taken. In this section, the method to design the avoidance manoeuvre developed in this paper is described. Specifically, it is considered that the avoidance actions will be taken with the deputy propulsive system, and is assumed that it has 3DOF control capability in translational control. Avoidance strategies are in general strongly dependent on the following aspects:

- **Nominal relative trajectory**: Different relative motion regime can influence the method of collision avoidance. For example, passively safe trajectory with E/I separation concept will exploit the geometry of relative motion to design manoeuvres that grants one-orbit minimum RN separation and if necessary a escape drift. On the other hand, complex forced motion fly-around require fast action and cannot in general establish passive safety with one-orbit minimum RN separation.

- **Severity of contingency**: Different level of contingency and failures may require different actions. For example, a mild contingency which can be recovered through at FDIR level might not require a avoidance manoeuvre which disrupt the nominal relative trajectory.

- **Recovery requirements**: Depending on the mission requirements, the evaporation of the relative motion formation may not be feasible for long time, or too costly to be recovered after the avoidance policy.

- **Autonomy requirements**: Promptness of the actions during operations will influence the need of the CAM planning algorithm to be executed onboard or performed with ground in the loop.

Options in literature have been explored for CAM strategies in relative orbits characterised by a level of E/I separation with analytic methods [27, 28] or pre-computed manoeuvres [29, 5] .

The method described in this paper focuses on avoidance problems in close-range, where complex forced motion trajectories are performed and a collision policy must be applied autonomously at the detection of a collision risk or contingency. Therefore, the requirement of computational efficiency of the CAM design algorithm is key to enable autonomous operations.Note that in this work, the avoidance region is considered larger than the geometrical KOZ defined around the chief objects. This allows to account for margin in navigation errors and actuation errors in the manoeuvres.

The CAM problem is here formulated as an optimisation problem which seeks to find the continuos control action in a short time interval after the collision risk detection which grants avoidance in the future with the chief object. The goal of this design is to introduce constraints in the optimisation problem which grants passive safety as defined in Section 3. This mean that the target conditions at the end of the CAM will grant PAS for the future uncontrolled trajectory evolution. The continuos control problem is discretised as shown in Figure 5, where the ROE trajectory is discretised and divided in two segment. The first segment shown in blue, denoted as ΔT_{CAM}, represents the time interval in which the CAM control action is provided. While the subsequent segment is additional time interval in which the segment is checked for collision with the chief avoidance region. The control accelerations u_i are considered constant over each segment.

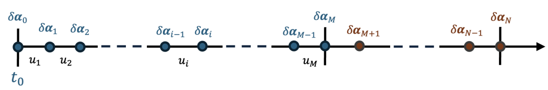

Fig. 5. Transcription of the continuos collision avoidance design problem.

To guarantee that the state $\delta\boldsymbol{\alpha}_N$ after the ΔT_{CHECK}, see Figure 5, guarantees a collision free trajectory without further control, the relative semi-major axis and relative longitude are considered as constraints. Particularly, the following constraints are enforced to guarantee escape:

$$\begin{cases} |\delta a_N| \geq A \\ -\text{sign}(\delta a_N)\delta\lambda_N \geq L \\ -\text{sign}(\delta a_N)\delta v_{T,N} \geq 0 \end{cases} \tag{12}$$

where δa_N and $\delta\lambda_N$ are the relative semi-major axis and the relative mean longitude of the node N, while

$\delta v_{T,N}$ is the relative velocity. In this way, the uncontrolled trajectory after $\delta\boldsymbol{\alpha}_N$ ensures a drift in along track motion that is always away from the chief object. The optimisation problem is then formulated as follows:

$$\min_{\mathbf{u}(t)} \quad \int_{t_0}^{t_N} u(\tau)d\tau \tag{13a}$$

$$\text{s.t.} \quad \delta\boldsymbol{\alpha}(t) = \Phi_{0,t}\delta\boldsymbol{\alpha}_0 + \int_{t_0}^{t} \Phi_{t,\tau}\mathrm{B}(\tau)\mathbf{u}(\tau)d\tau \tag{13b}$$

$$\delta\boldsymbol{\alpha}(t_0) = \delta\boldsymbol{\alpha}_0 \tag{13c}$$

$$\|\delta\mathbf{r}\|_2 \geq R_{KOZ} \tag{13d}$$

$$|\delta a_N| \geq A \tag{13e}$$

$$-\operatorname{sign}(\delta a_N)\delta\lambda_N \geq L \tag{13f}$$

$$-\operatorname{sign}(\delta a_N)\delta v_{T,N} \geq 0 \tag{13g}$$

$$\|\mathbf{u}(t)\|_\infty \leq U_{max} \tag{13h}$$

The cost function models the fuel optimality of the CAM scenario. The constraints include the system dynamics and initial conditions (Eqs. 13b and 13c), the avoidance of the KOZ throughout the scenario (Eq. 13d), and conditions on $\delta\boldsymbol{\alpha}_N$ to ensure that the trajectory does not collide with the chief after t_N. Finally, Eq. 13h limits the available acceleration according to the deputy's propulsion capabilities. The continuous control problem formulated in this way results in a challenging nonlinear optimization task, particularly for autonomous systems where efficiency is critical. In fact, constraints 13d–13g are non-convex, which makes them difficult to handle robustly within a Nonlinear Programming (NLP) framework. To overcome this, convexification techniques are adopted to reformulate the problem into an efficient optimization form suitable for onboard implementation. Specifically, constraints 13e–13g are highly non-convex and could, in principle, be addressed within a Mixed-Integer Nonlinear Programming (MINLP) formulation. However, MINLP problems are computationally expensive and generally unsuitable for real-time autonomous operations. In this work, convexification is achieved by considering half-space relaxations of the constraints, tailored to the initial conditions. For example, the constraint in Eq. 13e on the relative semi-major axis of the final state is reformulated by restricting it to the appropriate half-space of the absolute value inequality, depending on the sign of $\delta\boldsymbol{\alpha}_0$. The resulting expression then becomes:

$$\operatorname{sign}(\delta\boldsymbol{\alpha}_0)\delta\boldsymbol{\alpha}_N > A \tag{14}$$

This assumptions and convexification method is based on the fact that less delta-v will be required by the manoeuvres, and further more analysis on the solutions of the general NLP was conducted to validate this assumption. In the same way, the constraints in Equations 13f and 13g are limited to half-spaces depending on the conditions selected for Equation 13e. To deal with the nonconvexities present in Equation 13d regarding the KOZ avoidance the method of Sequential Convex Programming (SCP) is employed, where the optimisation problem is solved iteratively linearising the non-convex terms around the previous iterate solutions until convergence is reached. The subproblem in each iteration are solved with the dual-simplex algorithm of MATLAB linprog function, and an hard-trust region constraint is introduced to guarantee convergence to feasible solutions.

The CAM algorithm is tested on a scenario depicted in Table 3, where J_2 and differential drag are not accounted for. Note that the addition of these perturbations is straightforward from a modelling point of view through the STM of reference [34]. However, for such short scenario of optimisation problem the effects remain negligible. Moreover adding the differential drag perturbation will cause the considerations of the future avoidance of the state $\delta\boldsymbol{\alpha}_N$ to be tailored. In fact, depending on the ballistic coefficient, the differential drag will cause a drift in the trajectory in along-track, and the direction of escape should thus be defined accordingly in order to account for the fact that after the collision policy differential drag does not bring the deputy back in the vicinity of the chief [46].

Table 3. Parameters for the text case analysed in the CA scenario in proximity operations.

Parameter	Value
$\delta\boldsymbol{r}_0$	[-12, -3, -4] m
$\delta\boldsymbol{v}_0$	[+0.1, -0.03, +0.01] m/s
R_{KOZ}	10 m
ΔT_{CAM}	3 min
ΔT_{CHECK}	24 min (1/4 period)
M	19
N	71
$a_c A$	20 m
$a_c L$	20 m
U_{max}	2.5e-3 m/s^2
a_c	6913100 m
u_0	4 rad

Figure 6 shows the CAM trajectory designed for this scenario, displaying in blue the active collision policy segment, in dark red the check segment, in black the natural evolution of the relative trajectory after $\delta\boldsymbol{\alpha}_N$ and in gray the initial trajectory in collision course with the chief. From the RT projection of the trajectory shown on the bottom plot of Figure 6 it can be noted how the uncontrolled trajectory after the $\delta\boldsymbol{\alpha}_N$ successfully escape from the vicinity of the chief.

Figure 7 displays the control policy during the CAM segment resulting in 0.144 m/s cost, showcasing the use of only in-plane accelerations to reach the required conditions. Note that this property is in general common for many initial conditions which do not require a out-of-plane corrections to avoid the KOZ during the CAM and CHECK segments. Finally Figure 8 shows the Euclidean distance of the deputy and target during the whole CAM scenario, showcasing the feasibility of avoidance of the KOZ.

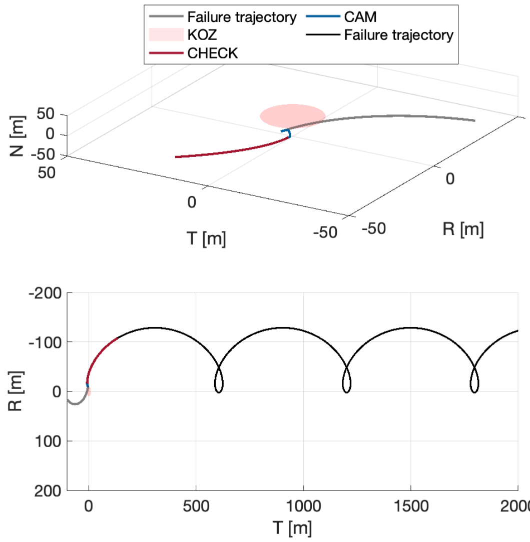

Fig. 6. CAM trajectory for the test case analysed in the chief centred RTN frame (top) and in the RT plane (bottom). Spherical avoidance zone is displayed in light red.

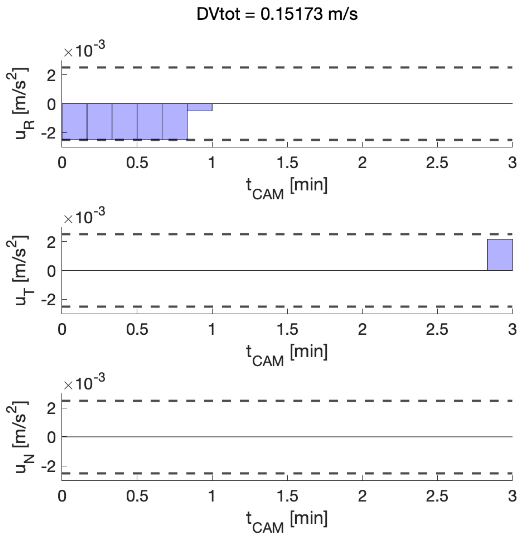

Fig. 7. CAM acceleration in RTN over the ΔT_{CAM} segment of the scenario analysed.

Upon preliminary simulations and testing on different initial conditions, the solution of the SCP problem is obtained in 4-8 iterations with around 100-200 ms of runtime on a laptop. Indeed situations in which an avoidance is not reachable are possible if the initial conditions shows a too large velocity which cannot be compensated in the defined ΔT_{CAM}. However, proximity operations are usually defined and designed to limit the approach velocity particular at the close-range and information on the capability to escape within certain velocity ranges can be used as constraint in the design of

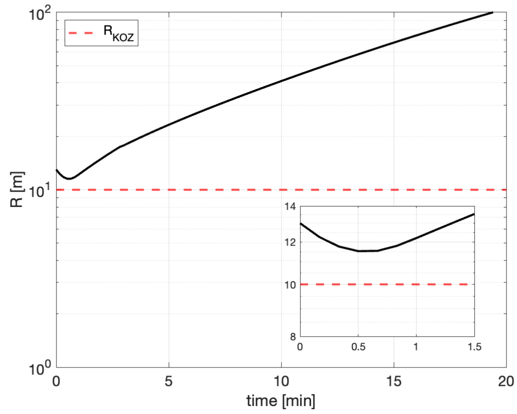

Fig. 8. Euclidean distance between the chief and deputy during the CAM scenario. The radius of the spherical avoidance region is displayed with the red dashed line.

the nominal trajectory, as done in reference [37].

6. Conclusions

Methods for assessing collision risk and planning avoidance manoeuvrers are essential to enabling autonomy in proximity operations. In this work, novel approaches are introduced to estimate the instantaneous collision probability of relative trajectories, while accounting for the limited computational resources available in autonomous applications. The proposed methods are tested on representative scenarios and compared against numerical collision probability calculations and Monte Carlo simulations. In addition, an avoidance algorithm based on convex optimization is presented for the rapid execution of manoeuvrers to escape from the chief satellite in the event of a close range contingency. Future research will focus on exploring advanced moment matching techniques to better characterize instantaneous collision probability from the relative position distribution, as well as testing the avoidance planning algorithms across a wider range of proximity operation scenarios.

Acknowledgments

This work was carried out within the Space It Up! project funded by the Italian Space Agency (ASI) and the Italian Ministry of University and Research (MUR) under contract No. 2024-5-E.0, CUP No. I53D24000060005.

References

[1] National Aeronautics and Space Administration (NASA), "In-Space Servicing, Assembly, and Manufacturing (ISAM)," `https://www.nasa.gov/nexis/isam/`, 2025, Accessed: 2025-08-21.

[2] Vavrina, M. A., Skelton, C. E., Deweese, K. D., Naasz, B. J., Gaylor, D. E., and D'Souza, C., "Safe

Rendezvous Trajectory Design for the Restore-L Mission," *Advances in the Astronautical Sciences*, 2019, pp. 3649–3668.

[3] Yamamoto, T., Matsumoto, J., Okamoto, H., Yoshida, R., Hoshino, C., and Yamanaka, K., "Pave the way for active debris removal realization: Jaxa commercial removal of debris demonstration (crd2)," *8th European Conference on Space Debris*, 2021, p. 200.

[4] Biesbroek, R., Aziz, S., Wolahan, A., Cipolla, S.-f., Richard-Noca, M., and Piguet, L., "The clearspace-1 mission: ESA and clearspace team up to remove debris," *Proc. 8th European Conference on Space Debris*, 2021.

[5] Vasconcelos, J., Gaggi, S., Amaral, T., Bakouche, C., Cotuna, A., and Friaças, A., "Close-Proximity Operations Design, Analysis, and Validation for Non-Cooperative Targets with an Application to the ClearSpace-1 Mission," *Aerospace*, Vol. 12, No. 1, 2025.

[6] European Space Agency (ESA), "ESA to build first in-orbit servicing mission with D-Orbit (RISE)," `https://www.esa.int/Space_Safety/ESA_to_build_first_in-orbit_servicing_mission_with_D-Orbit`, Oct. 2024, Accessed: 2025-08-21.

[7] Blackerby, C., Okamoto, A., Iizuka, S., Kobayashi, Y., Fujimoto, K., Seto, Y., Fujita, S., Iwai, T., Okada, N., Forshaw, J., et al., "The ELSA-d end-of-life debris removal mission: preparing for launch," *Proceedings of the International Astronautical Congress (IAC)*, 2019.

[8] "SpaceLogistics – In-Orbit Satellite Servicing | Northrop Grumman - MEV vehicles," `https://www.northropgrumman.com/what-we-do/space/space-logistics-services`, 2025, Accessed: 2025-09-09.

[9] "OrbitFab Website," `https://www.orbitfab.com/`, 2018, Accessed: 2025-09-09.

[10] D'Amico, S. and Montenbruck, O., "Proximity Operations of Formation-Flying Spacecraft Using an Eccentricity/Inclination Vector Separation," *Journal of Guidance, Control, and Dynamics*, Vol. 29, No. 3, 2006, pp. 554–563.

[11] Chan, F. K., *Spacecraft Collision Probability*, Aerospace Press, El Segundo, CA, 2008.

[12] Foster, J. L. and Estes, H. S., "A Parametric Analysis of Orbital Debris Collision Probability and Maneuver Rate for Space Vehicles," Technical report, NASA Johnson Space Center, 1992.

[13] Alfriend, K. T., Akella, M. R., Frisbee, J., Foster, J. L., Lee, D.-J., and Wilkins, M., "Probability of Collision Error Analysis," *Space Debris*, Vol. 1, No. 1, March 1999, pp. 21–35.

[14] Akella, M. R. and Alfriend, K. T., "Probability of Collision Between Space Objects," *Journal of Guidance, Control, and Dynamics*, Vol. 23, No. 5, 2000, pp. 769–772.

[15] Patera, R. P., "General Method for Calculating Satellite Collision Probability," *Journal of Guidance, Control, and Dynamics*, Vol. 24, No. 4, 2001, pp. 716–722.

[16] Serra, R., Arzelier, D., Joldes, M., and Rondepierre, A., "Probabilistic Collision Avoidance for Long-term Space Encounters via Risk Selection," *Advances in Aerospace Guidance, Navigation and Control*, edited by J. Bordeneuve-Guibé, A. Drouin, and C. Roos, Springer International Publishing, Cham, 2015, pp. 679–698.

[17] Krier, G., "Satellite Collision Probability for Long-Term Encounters and Arbitrary Primary Satellite Shape," *Proceedings of the 7th European Conference on Space Debris*, edited by T. Flohrer and F. Schmitz, Vol. 7, European Space Agency (ESA), ESA Space Debris Office, Darmstadt, Germany, 2017, p. n/a.

[18] Zhang, S., Fu, T., Chen, D., and Cao, H., "Satellite Instantaneous Collision Probability Computation Using Equivalent Volume Cuboids," *Journal of Guidance, Control, and Dynamics*, Vol. 43, No. 9, 2020, pp. 1757–1763.

[19] Pavanello, Z., Pirovano, L., and Armellin, R., "Long-Term Fuel-Optimal Collision Avoidance Maneuvers with Station-Keeping Constraints," *Journal of Guidance, Control, and Dynamics*, Vol. 47, No. 9, 2024, pp. 1855–1871.

[20] Campbell, M., "Collision monitoring within satellite clusters," *IEEE Transactions on Control Systems Technology*, Vol. 13, No. 1, 2005, pp. 42–55.

[21] Vaughan, R. M., Bergmann, E. V., and Walker, B. K., "Collision detection for spacecraft proximity operations," *Journal of Guidance, Control, and Dynamics*, Vol. 14, No. 2, 1991, pp. 225–229.

[22] Wang, Y., Bai, Y., Xing, J., Radice, G., Ni, Q., and Chen, X., "Equal-collision-probability-curve method for safe spacecraft close-range proximity maneuvers," *Advances in Space Research*, Vol. 62, No. 9, 2018, pp. 2599–2619.

[23] Slater, G. L., Byram, S. M., and Williams, T. W., "Collision Avoidance for Satellites in Formation Flight," *Journal of Guidance, Control, and Dynamics*, Vol. 29, No. 5, 2006, pp. 1140–1146.

[24] Larsson, R., Mueller, J., Thomas, S., Jakobsson, B., and Bodin, P., "Orbit Constellation Safety on the PRISMA In-Orbit Formation Flying Testbed," *Proceedings of the 3rd International Symposium on Formation Flying, Missions and Technologies*, 2008.

[25] Gaias, G. and Ardaens, J.-S., "Design challenges and safety concept for the AVANTI experiment," *Acta Astronautica*, Vol. 123, 2016, pp. 409–419, Special Section: Selected Papers from the International Workshop on Satellite Constellations and Formation Flying 2015.

[26] Núñez Garzón, U. E. and Lightsey, E. G., "Relating Collision Probability and Separation Indicators in Spacecraft Formation Collision Risk Analysis," *Journal of Guidance, Control, and Dynamics*, Vol. 45, No. 3, 2022, pp. 517–532.

[27] Koenig, A. W. and D'Amico, S., "Robust and Safe N-Spacecraft Swarming in Perturbed Near-Circular Orbits," *Journal of Guidance, Control, and Dynamics*, Vol. 41, No. 8, 2018, pp. 1643–1662.

[28] Kruger, J. J., Guffanti, T., Park, T. H., Murray-Cooper, M., Low, S. Y., Bell, T., D'Amico, S., Roscoe, C. W., and Westphal, J., *Adaptive End-to-End Architecture for Autonomous Spacecraft Navigation and Control During Rendezvous and Proximity Operations*.

[29] Borelli, G., Gaias, G., Colombo, C., Capuano, V., Urban, D., and Pulcino, V., "Safety Concept of Proximity Operations in Low Earth Orbit: The Sp-Eye Mission," *Proceedings of 76th International Astronautical Congress*, Sydney, Australia, 2025.

[30] Mueller, J. B. and Larsson, R., "Collision Avoidance Maneuver Planning with Robust Optimization," *Proceedings of the 7th International ESA Conference on Guidance, Navigation & Control Systems*, 2008.

[31] Pavanello, Z., De Maria, L., De Vittori, A., Maestrini, M., Di Lizia, P., and Armellin, R., "CAMmary: A review of spacecraft collision avoidance manoeuvre design methods," *Acta Astronautica*, Vol. 236, 2025, pp. 770–789.

[32] Sullivan, J., Grimberg, S., and D'Amico, S., "Comprehensive Survey and Assessment of Spacecraft Relative Motion Dynamics Models," *Journal of Guidance, Control, and Dynamics*, Vol. 40, No. 8, 2017, pp. 1837–1859.

[33] Gates, C. R., "A Simplified Model of Midcourse Maneuver Execution Errors," Technical Report Technical Report No. 32-504, Jet Propulsion Laboratory, 1963.

[34] Gaias, G., Ardaens, J.-S., and Montenbruck, O., "Model of J_2 perturbed satellite relative motion with time-varying differential drag," *Celestial Mechanics and Dynamical Astronomy*, Vol. 123, No. 4, Dec 2015, pp. 411–433.

[35] Gaias, G. and Lovera, M., "Trajectory Design for Proximity Operations: The Relative Orbital Elements' Perspective," *Journal of Guidance, Control, and Dynamics*, Vol. 44, No. 12, 2021, pp. 2294–2302.

[36] Borelli, G., Gaias, G., and Colombo, C., "Rendezvous and proximity operations design of an active debris removal service to a large constellation fleet," *Acta Astronautica*, Vol. 205, 2023, pp. 33–46.

[37] Borelli, G., Gaias, G., and Colombo, C., "Safe Guidance Scheme for Proximity Operations Forced Motion," *Journal of Guidance, Control, and Dynamics*, Vol. 48, No. 2, 2025, pp. 340–357.

[38] Clean Space, "Safe Close Proximity Operations," Tech. Rep. ESA-TECSYE-TN-010228, European Space Agency, 2018.

[39] Imhof, J. P., "Computing the distribution of quadratic forms in normal variables," *Biometrika*, Vol. 48, No. 3-4, 12 1961, pp. 419–426.

[40] Davies, R. B., "Algorithm AS 155: The Distribution of a Linear Combination of $\chi 2$ Random Variables," *Journal of the Royal Statistical Society. Series C (Applied Statistics)*, Vol. 29, No. 3, 1980, pp. 323–333.

[41] Zhang, H., Shen, J., and Wu, Z., "A Fast and Accurate Approximation to the Distributions of Quadratic Forms of Gaussian Variables," *Journal of Computational and Graphical Statistics*, Vol. 31, No. 1, Jan. 2022, pp. 304–311.

[42] Liu, H., Tang, Y., and Zhang, H. H., "A new chi-square approximation to the distribution of non-negative definite quadratic forms in non-central normal variables," *Computational Statistics & Data Analysis*, Vol. 53, No. 4, 2009, pp. 853–856.

[43] Daniels, H. E., "Saddlepoint Approximations in Statistics," *The Annals of Mathematical Statistics*, Vol. 25, No. 4, 1954, pp. 631 – 650.

[44] Kuonen, D., "Saddlepoint Approximations for Distributions of Quadratic Forms in Normal Variables," *Biometrika*, Vol. 86, No. 4, 1999, pp. 929–935.

[45] Lugannani, R. and Rice, S. O., "Saddle point approximation for the distribution of the sum of independent random variables," *Advances in Applied Probability*, Vol. 12, 1980, pp. 475 – 490.

[46] Borelli, G., Gaias, G., Nakajima, Y., Colombo, C., Capuano, V., Saggiomo, F., Leccese, G., and Natalucci, S., "Mission analysis and guidance and control for the SpEye inspection CubeSat," *Acta Astronautica*, Vol. 220, 2024, pp. 75–87.